# Supplementary Methods

## Bioluminescence Imaging (BLI) Acquisition

In vivo bioluminescence imaging was performed on an IVIS50 (PerkinElmer; Living Image 3.2, 1min to 1sec exposure, bin8, FOV12.5cm, f/stop1, open filter). Mice were injected intraperitoneally with D-luciferin (150mg/kg in PBS; Gold Biotechnology) and imaged under isoflurane anesthesia (2% vaporized in O2). Total photon flux (photons/sec) was measured from fixed regions of interest (ROIs) over the heads of the mice using Living Image 2.6.

## Optical Intrinsic Signal (OIS) Imaging Acquisition

OIS imaging was performed per published protocols[1]. Briefly, mice were anesthetized with IP Ketamine-Xylazine (86.9 mg/kg Ketamine and 13.4 mg/kg Xylazine) and fixed in a custom-made head holder. Mouse body temperature was maintained at 37°C on a heating pad via rectal feedback (mTCII, Cell Microcontrols). Sequential illumination was provided at four wavelengths (478 nm, 588 nm, 610 nm, and 625 nm) by a ring of light emitting diodes (LEDs) placed approximately 10 cm above the mouse's head. Diffuse reflected light was collected using a lens (Vivitar Series 1, 85 mm, f/2.8) and a cooled, frame-transfer EMCCD camera (iXon 897, Andor Technologies, 512 × 512 pixels, 16 µm x 16 µm pixels) with 4x4 on-camera binning (i.e. 128 x 128 images) over a field of view of $1cm^2$. The LED ring and camera were time-synchronized and controlled via computer using custom-written software (MATLAB, Mathworks). The images were

acquired at a full frame rate of ~30 Hz, which is well above the heart and respiration rates (~10 and 2.5 Hz, respectively). Image sequences were collected for at least 10 min up to 45 min.

## Laser Speckle Contrast Imaging (LSCI) Acquisition

Measures of cerebral perfusion were performed as previously described[2]. Illumination was provided by a laser (690 nm, 39 mW diode, Thorlabs HL6738MG). LCSI incorporated the same camera and lens used for OIS collection but without binning (i.e. 512 × 512 images) and the lens' f/# adjusted to f/5.6 to adequately sample the laser speckle pattern[3,4]. Images were acquired at a full frame rate of 10 Hz, with an integration time of 10ms. 5-minute runs of images were collected at a time. At least 15 minutes of data was collected each imaging session. During imaging, mice were anesthetized and maintained at a body temperature of 37°C as during OIS imaging.

## OIS Data Processing

Changes in diffuse reflected light were converted to changes in hemoglobin concentration using the Modified Beer-Lambert Law as described previously[1]. Oxygenated hemoglobin exhibits the highest signal-to-noise and was used for all subsequent analyses. Ten to 45 minutes of data were analyzed for each mouse. Fluctuations in hemoglobin were temporally filtered from 0.009Hz to 0.08Hz per studies examining infraslow activity[1,5,6]. Data were then down-sampled from 30 Hz to 1 Hz using an anti-aliasing filter. The hemoglobin data was then smoothed with a Gaussian kernel with a full width half maximum (FWHM) = ~225 μm. To remove global sources of variance, the average signal from each brain hemisphere and a seed placed over the

sagittal sinus were simultaneously regressed from the data following previous methods[7] Lastly, the data and brain mask for each mouse were affine-transformed to a common atlas space by using bregma and lambda as landmarks.

## LCSI Data Processing

A relative index of instantaneous CBF was derived from speckle contrast measure using a 9 x 9 kernel as described[2]. The full resolution CBF image sequences (512 × 512 pixels) were spatially binned using a 4 × 4 kernel to 128 x 128 pixels to reduce noise and data set size. The CBF data was then low pass filtered (0.08 Hz) and down-sampled from 10 to 1 Hz. Lastly, CBF data was smoothed with a Gaussian kernel (FWHM = ~1.2 mm). The average CBF was then calculated for the hindlimb somatosensory right (tumor), hindlimb somatosensory left, visual right, and visual left seeds.

## Mouse MRI Acquisition

MRI data were collected on a 4.7T small animal MRI system (Agilent Technologies) using a laboratory-built, actively decoupled, volume-transmit/surface-receive coil configuration. Mice were anesthetized (0.8% isoflurane) and restrained in a three-point head holder for all data collection. T2-weighted, spin echo images were acquired using the following parameters: echo time/repetition time: 40/1250 msec; field of view: 16 x 16 $mm^2$; slice thickness: 1 mm; matrix size: 128 x 128; number of averages: 32; dummy scans: 2; and acquisition time: 17 min 4 sec.

## Human R-fMRI Data Preprocessing

R-fMRI data underwent preprocessing as described[8]. Briefly, this included: 1) compensation for asynchronous slice acquisition using sinc interpolation; 2) elimination of odd/even slice intensity differences resulting from interleaved acquisition; 3) whole brain intensity normalization to achieve a mode value of 1000; 4) spatial realignment within and across fMRI runs; and 5) resampling to 3mm cubic voxels in atlas space including realignment and atlas transformation in one resampling step. Cross-modal (e.g., T2-weighted to T1-weighted) image registration was accomplished by aligning image gradients[9]. Cross-modal image registration was manually checked for every subject.

Data underwent additional preprocessing steps: 6) temporal bandpass filtering, retaining frequencies between 0.01-0.1Hz, 7) removal of spurious variance through regression of 12 parameters of head motion (six parameters obtained by rigid body motion correction, as well as their derivatives), 2 ventricle regions of interest, and 2 white matter regions of interest, and 8) flagging of frames with a framewise displacement > 0.5mm to be excluded from the R-fMRI computations[10]. A shift mask was then generated by removing frames proceeding or after excluded frames. A minimum of 120 usable frames was required for subject inclusion. Thus, 3 out of 30 patients were excluded. In the retained data, on average, 402 out of 439 frames remained in the included patients.

## Human R-fMRI Lag Processing and Analysis

For every brain voxel, lag was calculated relative to the ‘homotopic’ reference voxel in the opposite hemisphere. The homotopic reference voxel was determined by flipping

about the X axis in atlas space. Lagged cross-correlation analysis was performed for each voxel over the range ±5 TRs (±2.2 seconds) as previously described[8]. (Fig. 8C):

$$C_i(\tau) = (\frac{1}{n_\tau}) \sum_t [\frac{r_i(t) \cdot s_i(t+\tau)}{\sigma_{s_i} \sigma_g}], \quad (2)$$

where $r_i$ is the homotopic reference signal, $s_i$ is the signal in voxel $i$, and $\sigma_{s_i}$ and $\sigma_g$ are the standard deviations of the two signals. The summation runs over frames indexed by $t$, and $n_\tau$ is the number of frames included after a shift of $\tau$ (-2.2s to +2.2s). To determine the shift that maximizes the cross-correlation function at a temporal resolution finer than 1TR, the lag ($\tau$) corresponding to the maximum of $C_i(\tau)$ was identified. $C_i(\tau)$ at this lag, as well as one step forward and backward, were fit with a parabolic function and the peak value, $C_i(\tau^m)$, and corresponding temporal shift ($\tau^m$) were computed[11]. Positive and negative values of $\tau^m$ correspond, respectively, to a lag or lead relative to the homotopic voxel signal. The lag measure, $\tau^m$, was computed for every voxel within the brain (with homotopic voxels necessarily assigned opposite values). Finally, lag values were smoothing using a 6mm FWHM smoothing kernel constrained by a brain mask.

# Supplementary References


1 White BR, Bauer AQ, Snyder AZ, *et al*. Imaging of Functional Connectivity in the Mouse Brain. *PLOS ONE* 2011; **6**: e16322.

2 Bergonzi KM, Bauer AQ, Wright PW, *et al*. Mapping functional connectivity using cerebral blood flow in the mouse brain. *J Cereb Blood Flow Metab* 2015; **35**: 367–370.

3 Dunn AK, Bolay H, Moskowitz MA, *et al*. Dynamic imaging of cerebral blood flow using laser speckle. *J Cereb Blood Flow Metab Off J Int Soc Cereb Blood Flow Metab* 2001; **21**: 195–201.

4 Boas DA, Dunn AK. Laser speckle contrast imaging in biomedical optics. *J Biomed Opt* 2010; **15**. doi:10.1117/1.3285504.

5 Fox MD, Raichle ME. Spontaneous fluctuations in brain activity observed with functional magnetic resonance imaging. *Nat Rev Neurosci* 2007; **8**: 700–711.

6 Cordes D, Haughton VM, Arfanakis K, *et al.* Frequencies Contributing to Functional Connectivity in the Cerebral Cortex in “Resting-state” Data. *Am J Neuroradiol* 2001; **22**: 1326–1333.

7 Bauer AQ, Kraft AW, Wright PW, *et al*. Optical imaging of disrupted functional connectivity following ischemic stroke in mice. *NeuroImage* 2014; **99**: 388–401.

8 Siegel JS, Snyder AZ, Ramsey L, *et al*. The effects of hemodynamic lag on functional connectivity and behavior after stroke. *J Cereb Blood Flow Metab Off J Int Soc Cereb Blood Flow Metab* 2016; **36**: 2162–2176.

9 Rowland DJ, Garbow JR, Laforest R, *et al*. Registration of [18F]FDG microPET and small-animal MRI. *Nucl Med Biol* 2005; **32**: 567–572.

10 Power JD, Barnes KA, Snyder AZ, *et al*. Spurious but systematic correlations in functional connectivity MRI networks arise from subject motion. *NeuroImage* 2012; **59**: 2142–2154.

11 Mitra A, Snyder AZ, Hacker CD, *et al*. Lag structure in resting-state fMRI. *J Neurophysiol* 2014; **111**: 2374–2391.

# Supplementary Figures

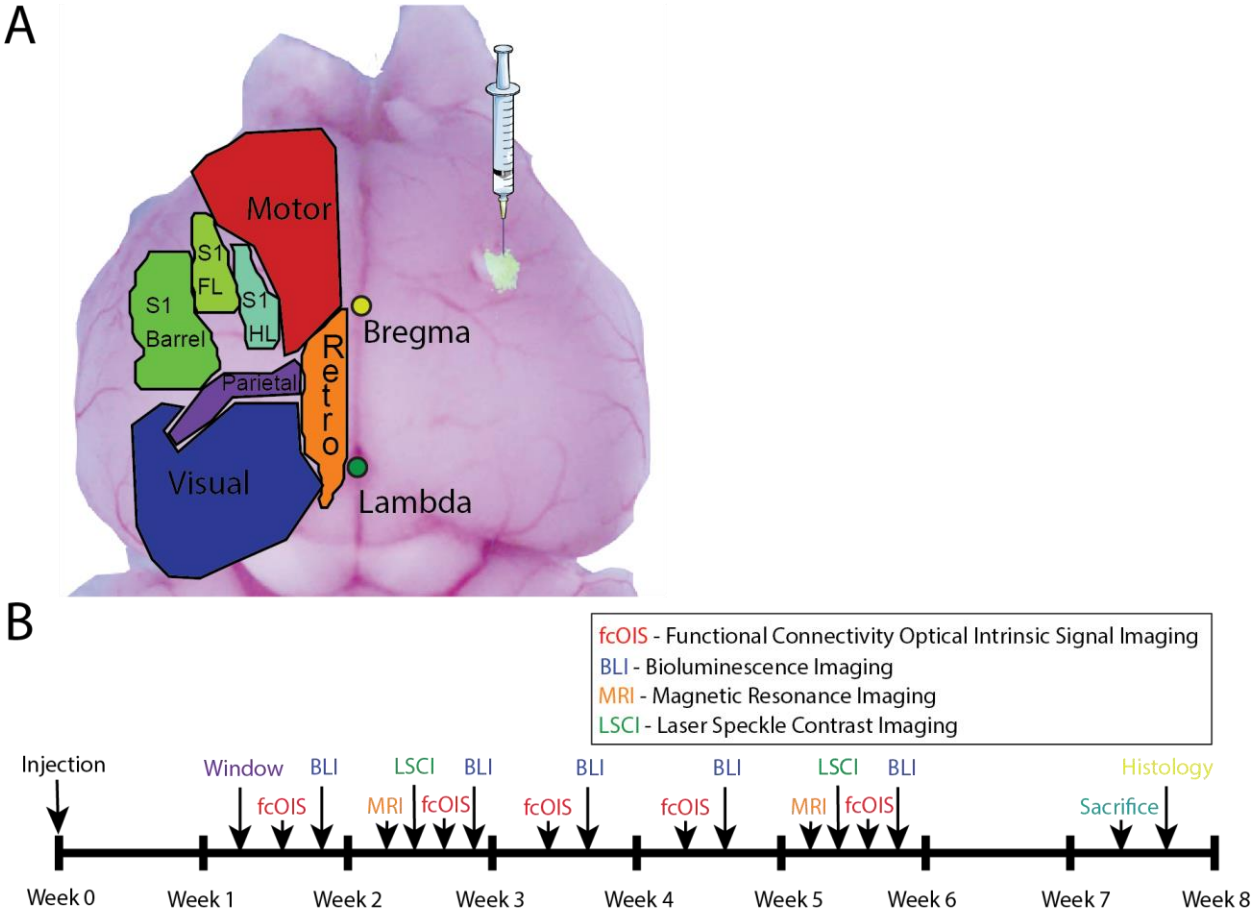


Fig. S1 – Injection site and timeline. A) Fluorescence image of a mouse brain injected with green fluorescent protein expressing glioblastoma cells. The fluorescent focus indicates the injection site – the right primary somatosensory forelimb cortex. A parcellation of the mouse brain using the Paxinos atlas is overlaid on the opposite hemisphere. B) Timeline of the experimental design. S1 FL – primary somatosensory forelimb cortex, S1 HL – primary somatosensory hindlimb cortex, S1 Barrel – primary somatosensory whisker barrel cortex, Retro – retrosplenial cortex.

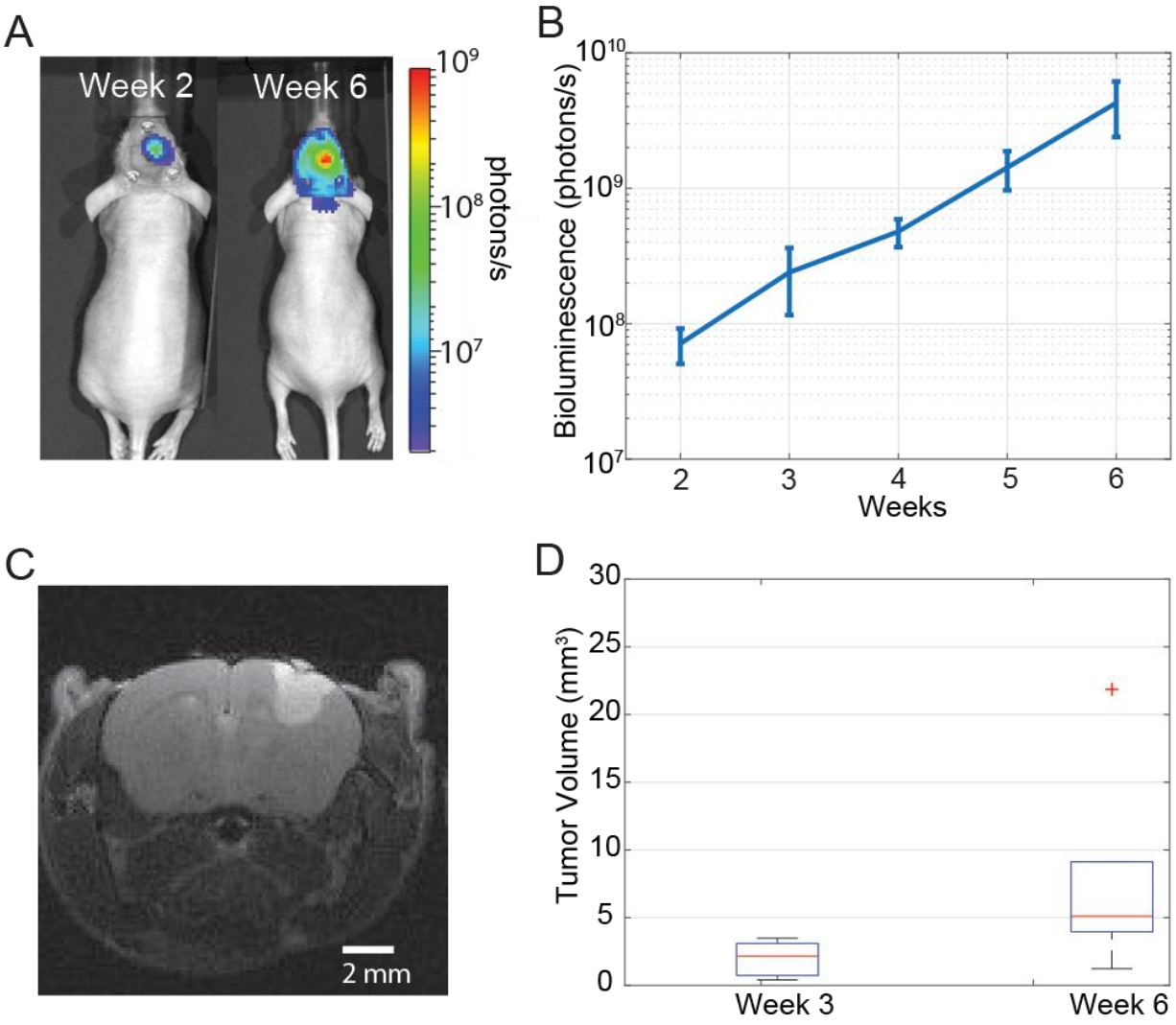


Fig. S2 – Tumor burden measurements. A) Bioluminescence images of a representative mouse injected with glioma cells at week 2 and week 6 post-injection. B) Quantification of average bioluminescence signal from mice injected with glioma cells (n=13) at different weeks. Plot indicates that there was a steady, exponential increase in tumor cells over the course of the experiment. C) T2-weighted MRI slice from a representative mouse injected with glioma cells. D) Box and whisker plot of tumor volumes at week 3 and week 6 post-injection for a subset of mice injected with glioma cells(n=6). Plot indicates that tumor volume increased over time.

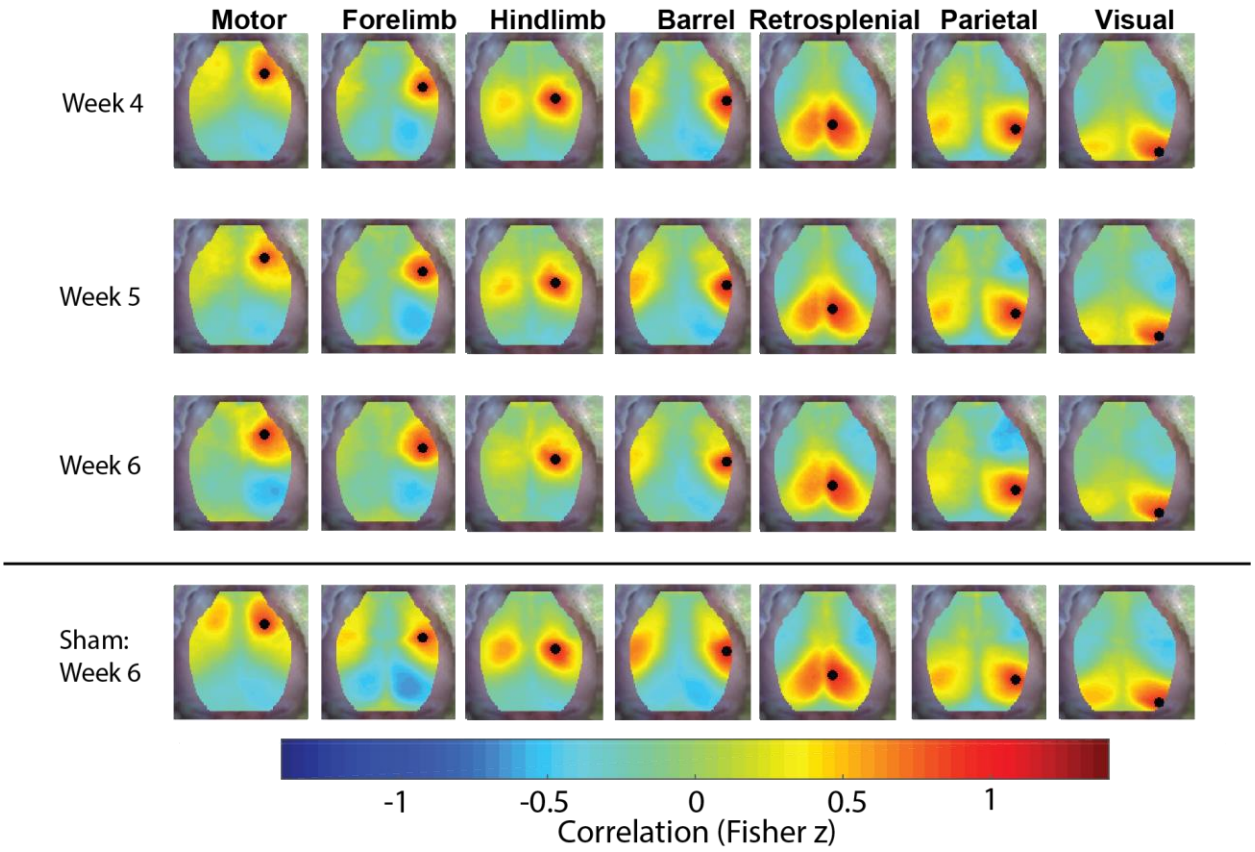


Fig. S3 – Glioma contralateral seed oxyhemoglobin FC maps. Group average functional connectivity maps constructed with oxygenated hemoglobin traces of mice injected with glioma cells (n=13) for the 4$^{th}$, 5$^{th}$ and 6$^{th}$ weeks post-injection. Group average functional connectivity maps of mice with sham injections (n=20) for the 6$^{th}$ week post-injection are included for reference. Only functional connectivity maps for seeds in the right hemisphere ipsilateral to the injection site are displayed. The black dots indicate the location of the seed used to construct the functional connectivity map. These functional connectivity maps show that there is a general loss of symmetry with the passage of time, which is consistent with the results from the functional connectivity maps constructed with seeds placed in the contralateral hemisphere.

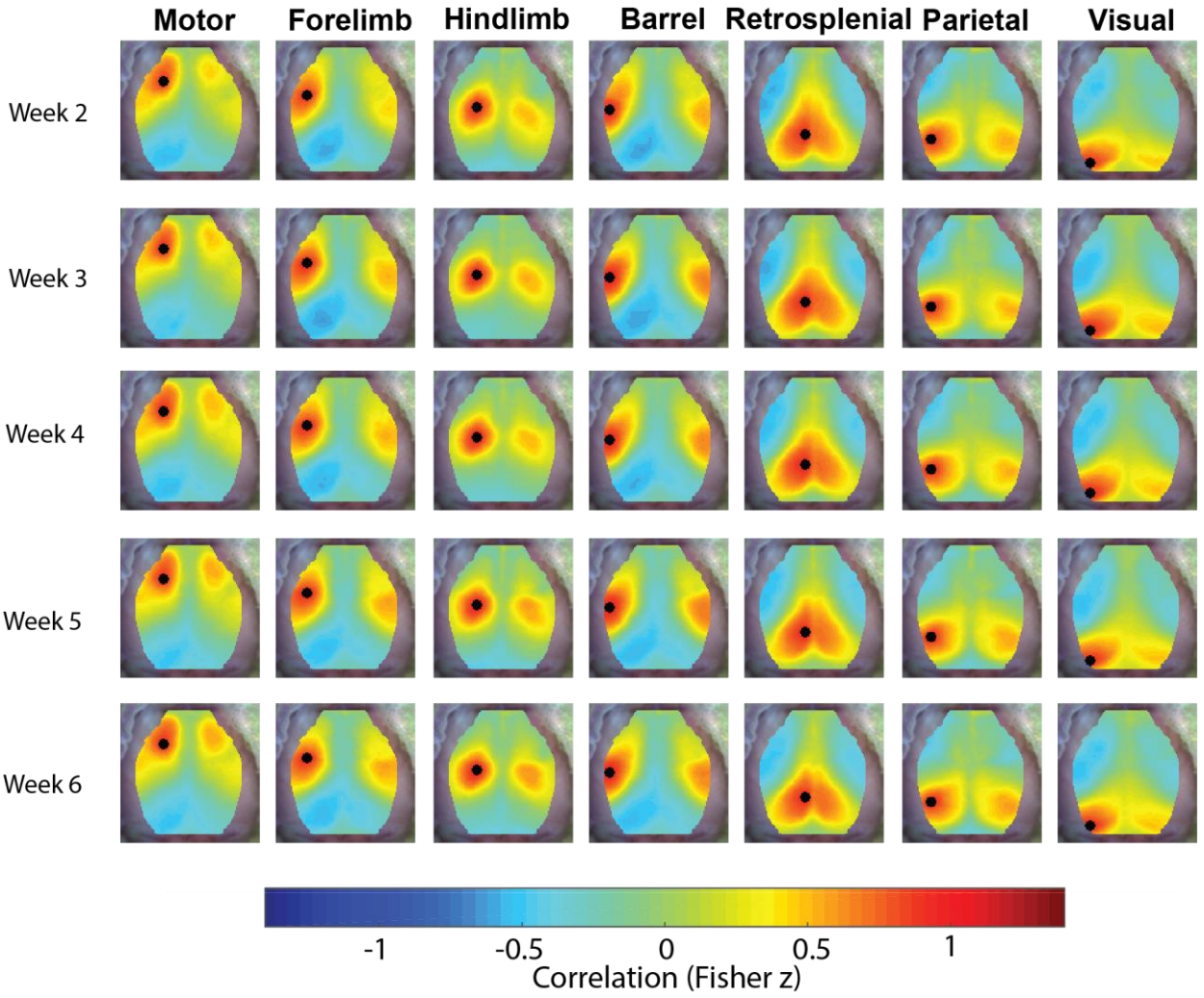


Fig. S4 – Sham contralateral seed oxyhemoglobin FC maps. Group average functional connectivity maps constructed with oxygenated hemoglobin traces of mice with sham injections (n=20) for the 2$^{nd}$ through 6$^{th}$ weeks post-injection. Only functional connectivity maps for seeds in the left hemisphere contralateral to the injection site are displayed. The black dots indicate the location of the seed used to construct the functional connectivity map. In general, the symmetry in these functional connectivity maps increase with the passage of time.

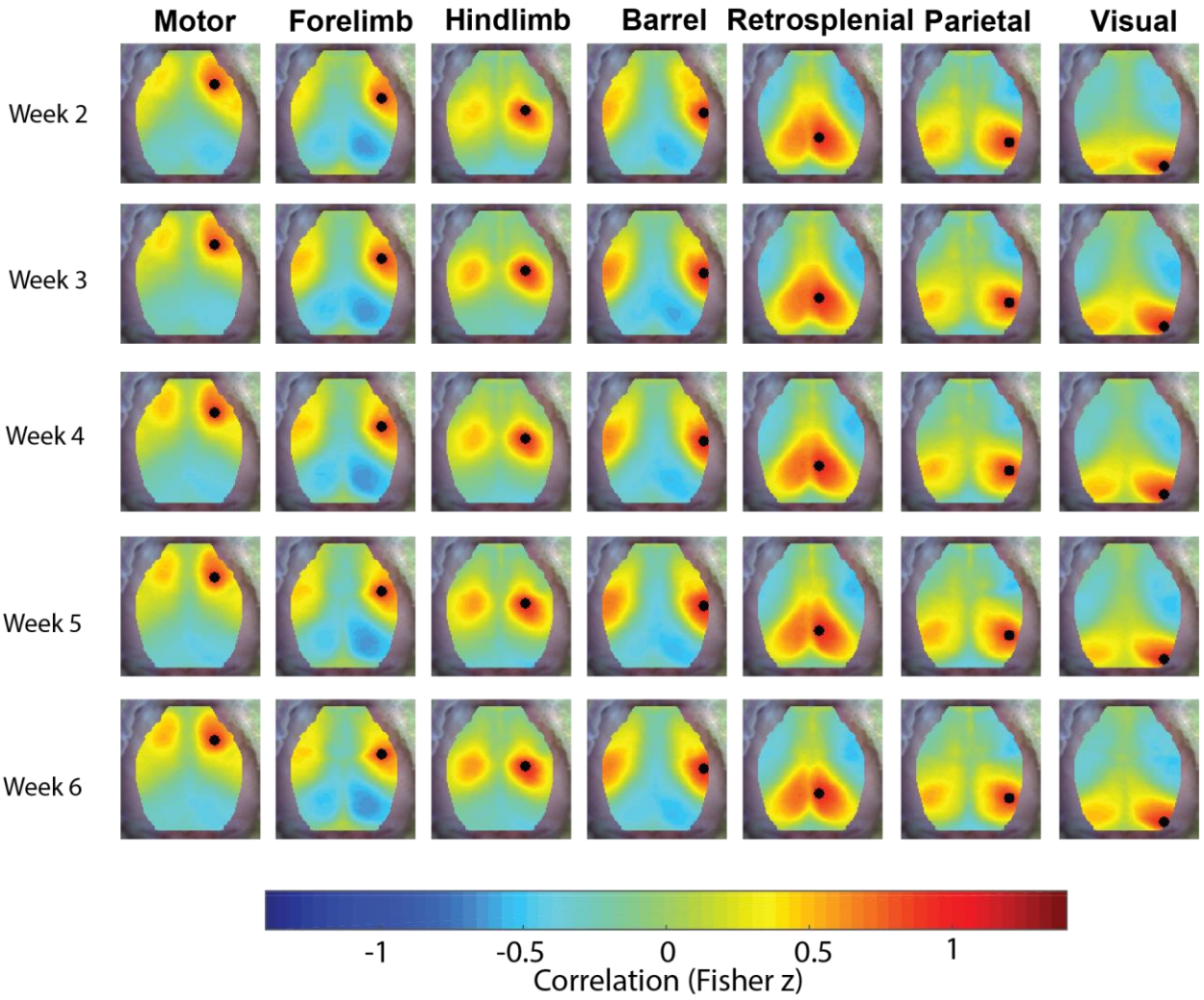


Fig. S5 – Sham ipsilateral seed oxyhemoglobin FC maps. Group average functional connectivity maps constructed with oxygenated hemoglobin traces of mice with sham injections (n=20) for the 2$^{nd}$ through 6$^{th}$ weeks post-injection. Only functional connectivity maps for seeds in the right hemisphere ipsilateral to the injection site are displayed. The black dots indicate the location of the seed used to construct the functional connectivity map. There is a general increase in the symmetry of these functional connectivity maps with the passage of time, which is consistent with the results from the functional connectivity maps constructed with seeds placed in the contralateral hemisphere.

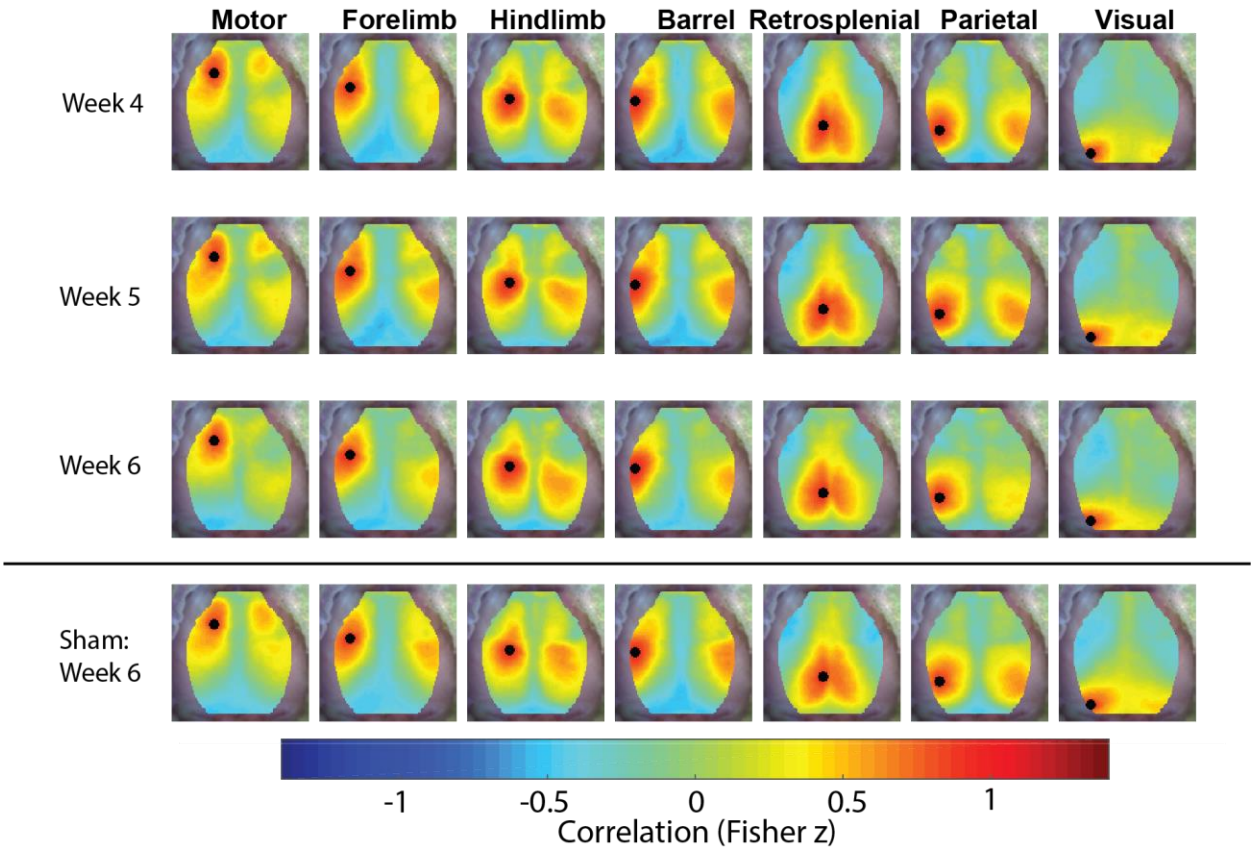


Fig. S6 – Glioma contralateral seed deoxyhemoglobin FC maps. Group average functional connectivity maps constructed with deoxygenated hemoglobin traces of mice injected with glioma cells (n=13) for the 4$^{th}$, 5$^{th}$ and 6$^{th}$ weeks post-injection. Group average functional connectivity maps of mice with sham injections (n=20) for the 6$^{th}$ week post-injection are included for reference. Only functional connectivity maps for seeds in the left hemisphere contralateral to the injection site are displayed. The black dots indicate the location of the seed used to construct the functional connectivity map. These functional connectivity maps show that there is a general loss of symmetry with the passage of time, which is consistent with the results from the functional connectivity maps constructed with oxygenated hemoglobin.

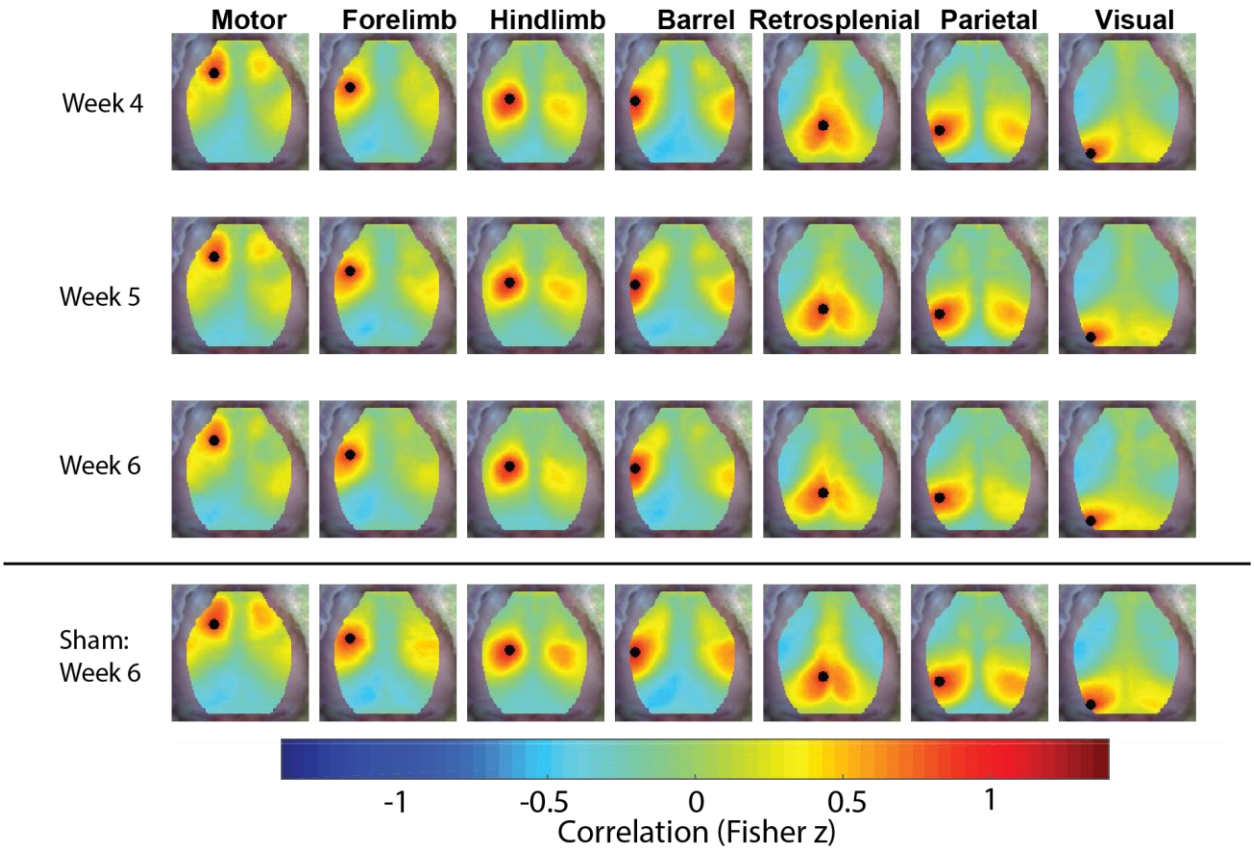


Fig. S7 – Glioma contralateral seed total hemoglobin FC maps. Group average functional connectivity maps constructed with total hemoglobin traces of mice injected with glioma cells (n=13) for the 4$^{th}$, 5$^{th}$ and 6$^{th}$ weeks post-injection. Group average functional connectivity maps of mice with sham injections (n=20) for the 6$^{th}$ week post-injection are included for reference. Only functional connectivity maps for seeds in the left hemisphere contralateral to the injection site are displayed. The black dots indicate the location of the seed used to construct the functional connectivity map. These functional connectivity maps show that there is a general loss of symmetry with the passage of time, which is consistent with the results from the functional connectivity maps constructed with either oxygenated or deoxygenated hemoglobin.

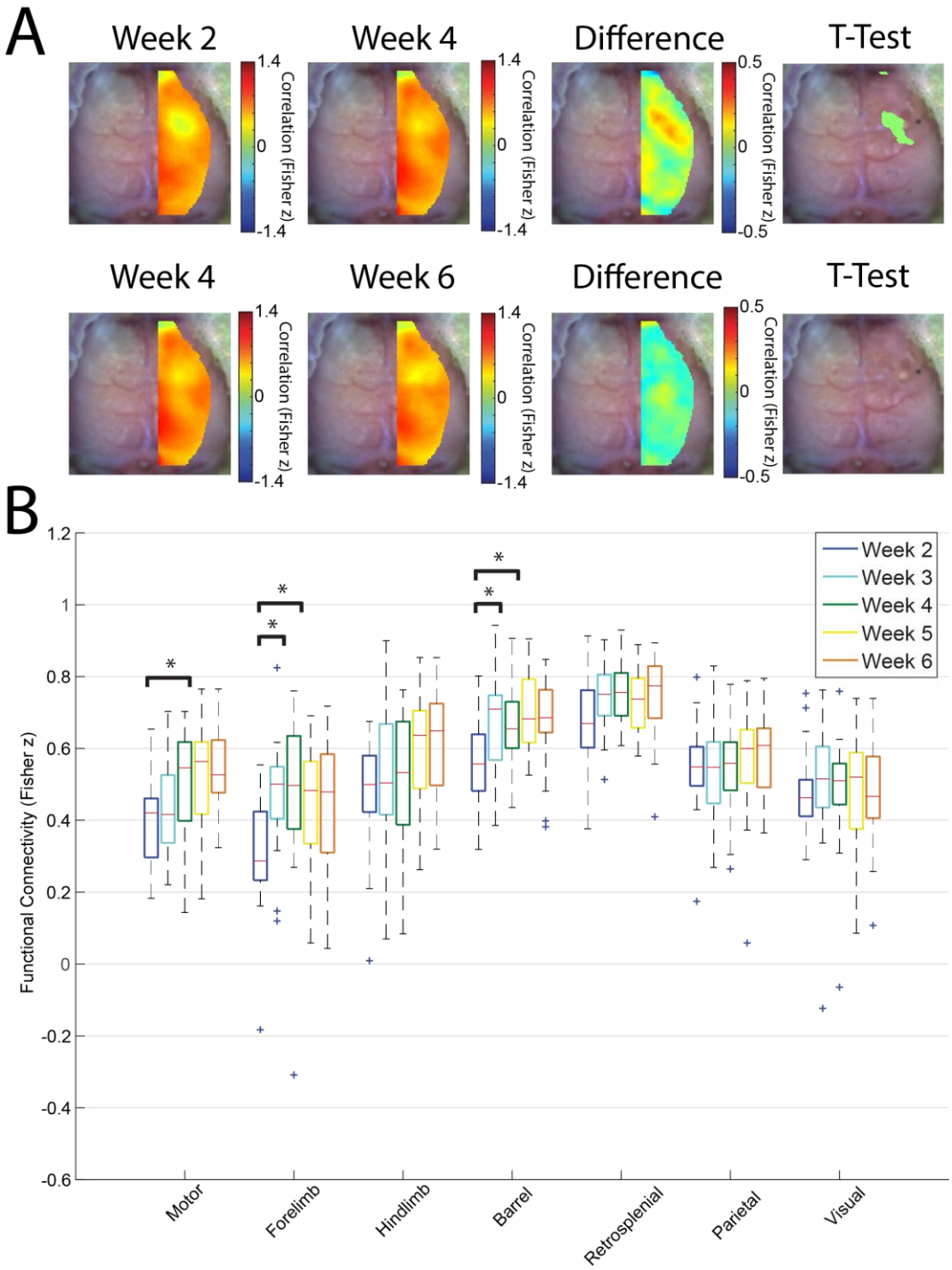


Fig. S8 – Homotopic connectivity metrics. A) Group average homotopic connectivity maps of mice injected with glioma cells (n=20) for different weeks. The 2nd week post-injection map, the 4th week post-injection map, and the difference and t-test (paired, $p<0.05$, FDR corrected) maps between the 2nd and 4th weeks post-injection are displayed on the top row. The 4th week post-injection map, the 6th week post-injection map, and the difference and t-test (paired, $p<0.05$, FDR corrected) maps between the

4th and 6th weeks post-injection are displayed on the bottom row. The maps show that functional connectivity near the injection increases during the early time points after injection and then remains stabled for the later time points. B) Quantification of group average homotopic connectivity of glioma injected mice (n=20) for seven homotopic seed pairs within our field of view (paired, * indicates p<0.05, Bonferroni corrected).

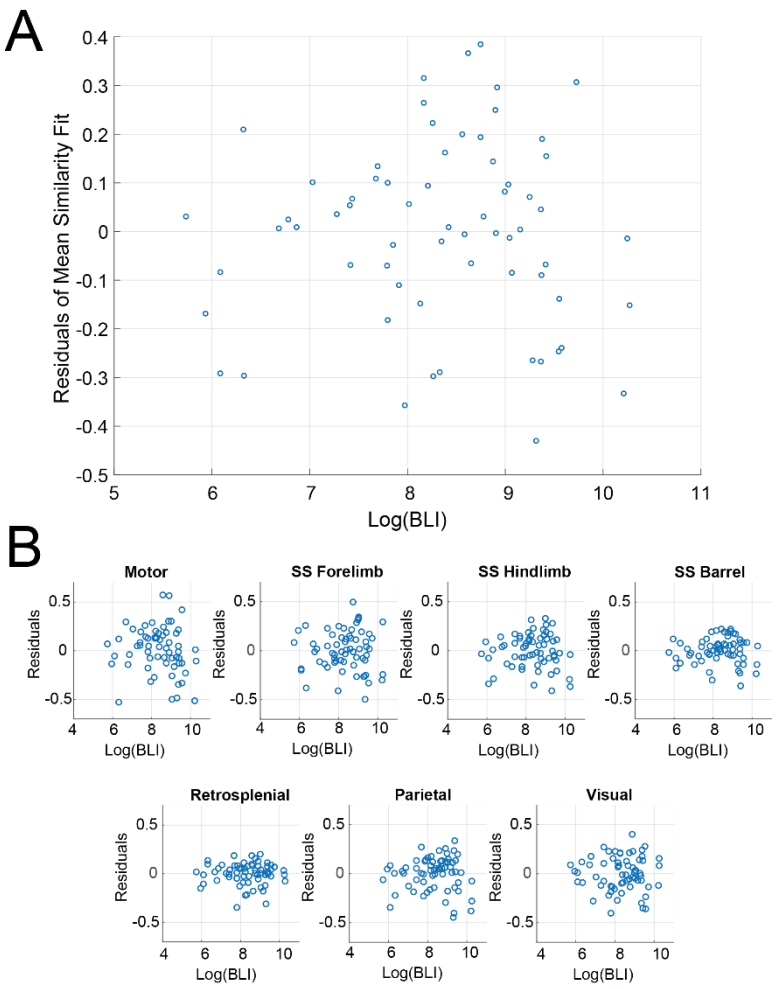


Fig. S9 – Residual Analysis. A) Residual of the linear fit between mean similarity across the cortex and bioluminescence imaging (BLI). B) Residual of the linear fit between homotopic connectivity (HC) and BLI. The residuals for both metric (mean similarity and HC) appear randomly distributed about zero suggesting that the linear regression model is valid.

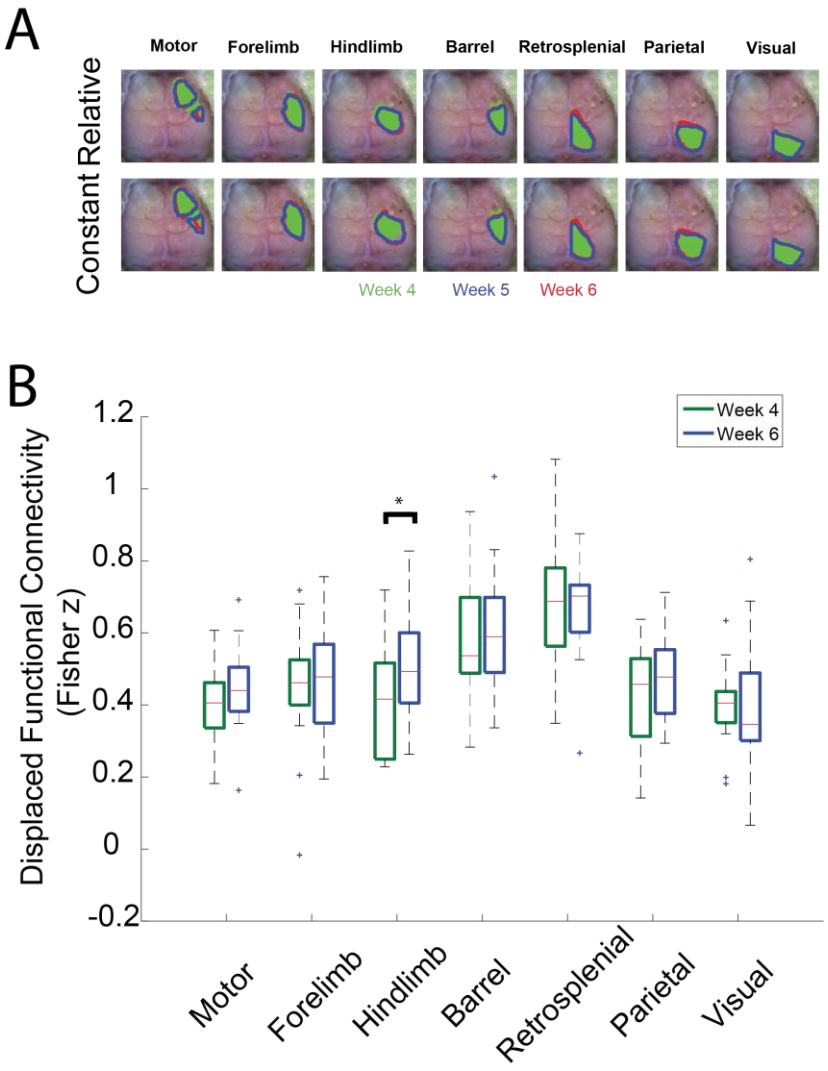


Fig. S10 – Functional connectivity contours and displaced functional connectivity. A) Group average functional connectivity contours of fifty percent of relative and constant maximums (n=20) for different weeks. Relative functional connectivity contours use a threshold based on fifty percent of the maximum of each week. Constant functional connectivity contours use a threshold based on fifty percent of the maximum at week 4 post injection. Green = Week 4, Red = Week 5, and Blue = Week 6. The contours for the sham injected mice are relatively stable compared to the glioma injected mice. B) Quantification of the group average displaced functional connectivity (n=20) for week 4 and week 6 post injection (* indicates $p<0.05$). Displaced functional connectivity is calculated by using the relative functional connectivity contours as regions of interest and averaging all the Fisher z correlation values within each contour. Only the hindlimb region had increased magnitude when accounting for displacement.

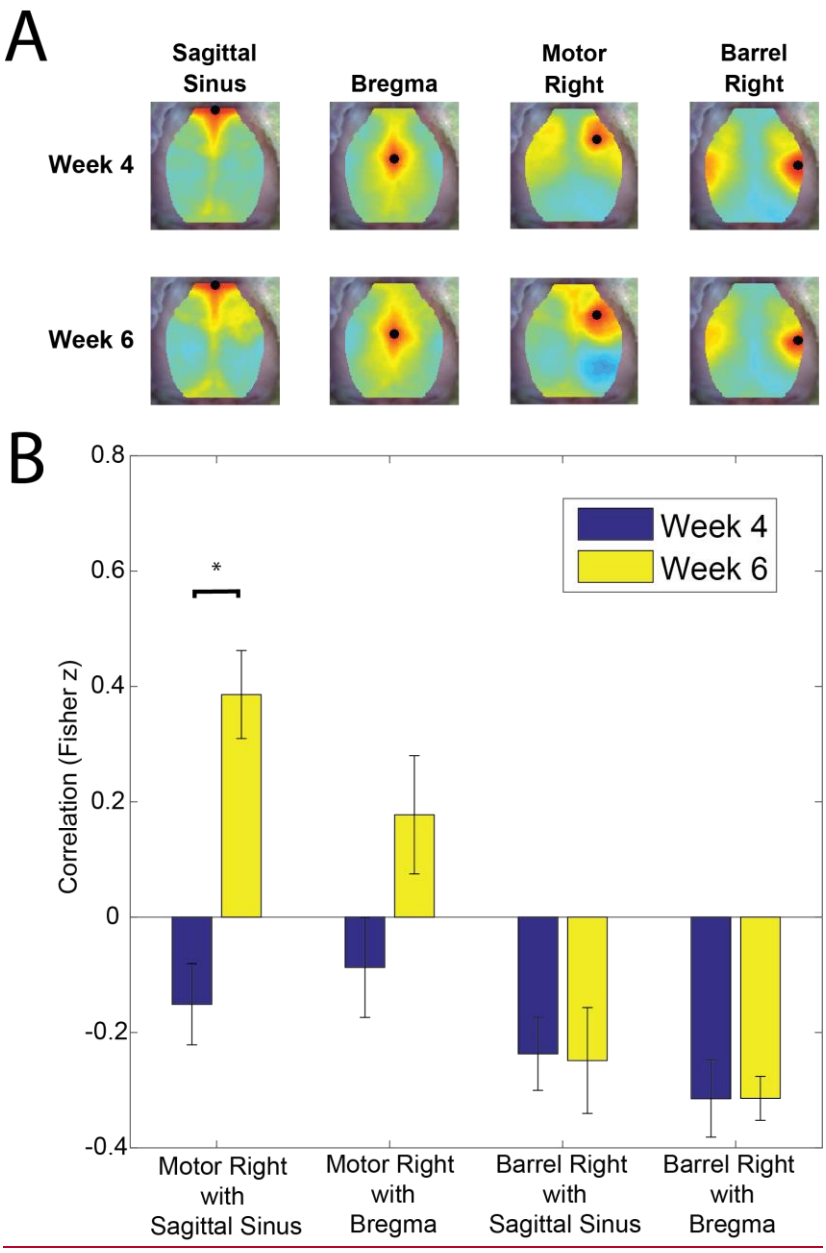


Fig. S11 – Extended vascular correlation analysis. Group average correlation maps (n=13) of sagittal sinus, bregma, motor right, and barrel right seeds at week 4 and week 6 post-injection. B) Quantification of the group average correlation (n=13) between the motor right seed and both sagittal sinus and bregma seeds and between the barrel right seed and both sagittal sinus and bregma seeds. Correlation between the motor right seed and the sagittal sinus significantly (p-value<0.05) increases with time suggesting that neurovascular uncoupling is occurring near motor right seed. The correlation between motor right seed and bregma substantially increases; but this increase is not significant, likely because there are hemodynamic lags between the anterior parts of the sagittal sinus and more posterior structures along midline and lack of power. The barrel

right seed does not become more correlated with the vascular seeds suggesting neurovascular coupling remains intact for the barrel right region.

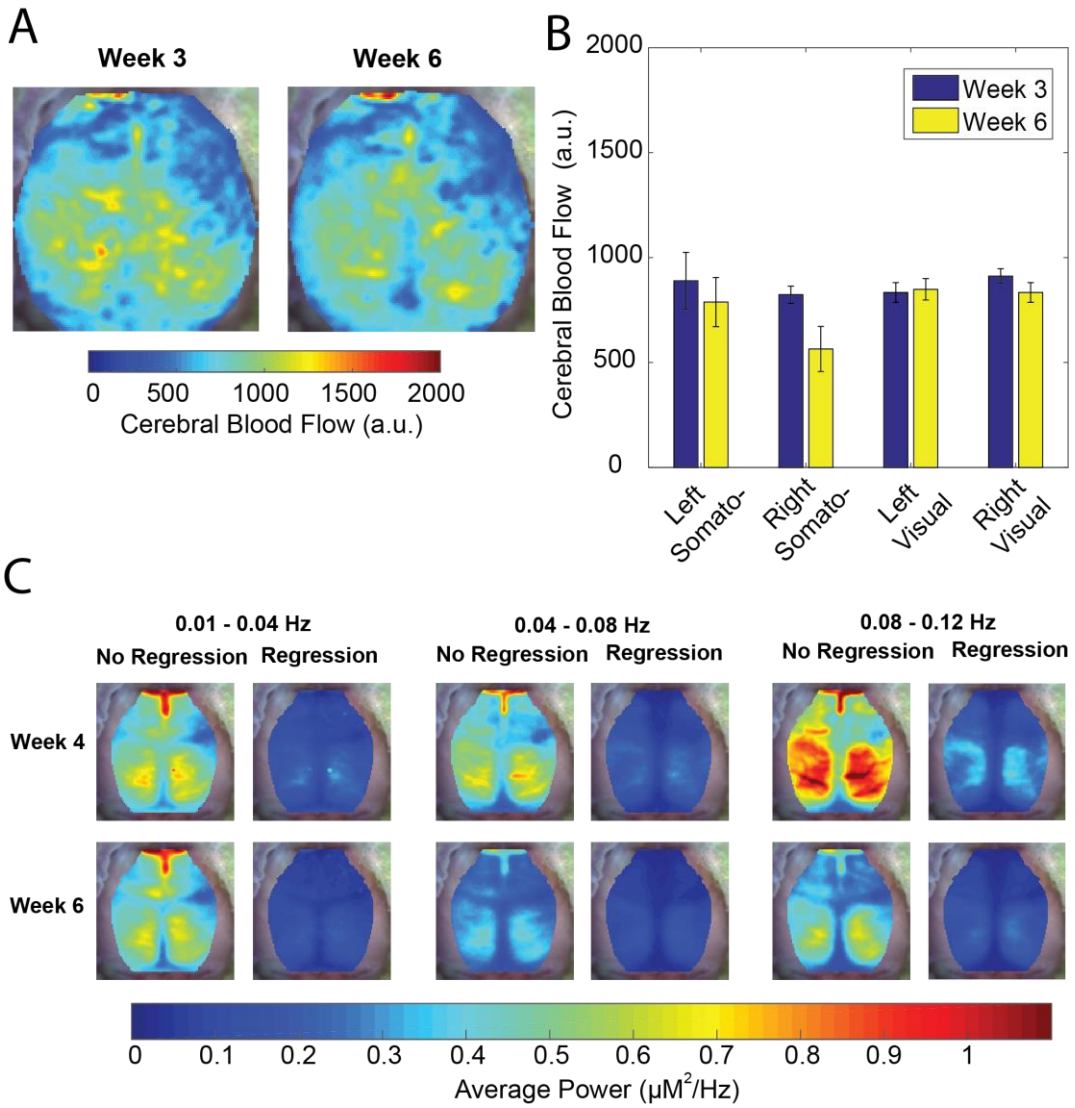


Fig. S12 – Hemodynamics in sham mice. A) Group average cerebral blood flow maps for a subset of sham mice (n=3) at week 3 and week 6 post injection. B) Quantification of the group average cerebral blood flow value (n=3) for the left and right somatosensory hindlimb and left and right visual seeds at week 3 and week 6 post-injection. This graph indicates that the blood flow in the assessed regions are unchanged as time passes. C) Group average power maps (n=15) for three frequency bands with and without regression of the signal from a vascular feature (sagittal sinus seed) at week 4 and week 6 post-injection. In general, average power maps decrease in magnitude as time progresses and with regression of the sagittal sinus.

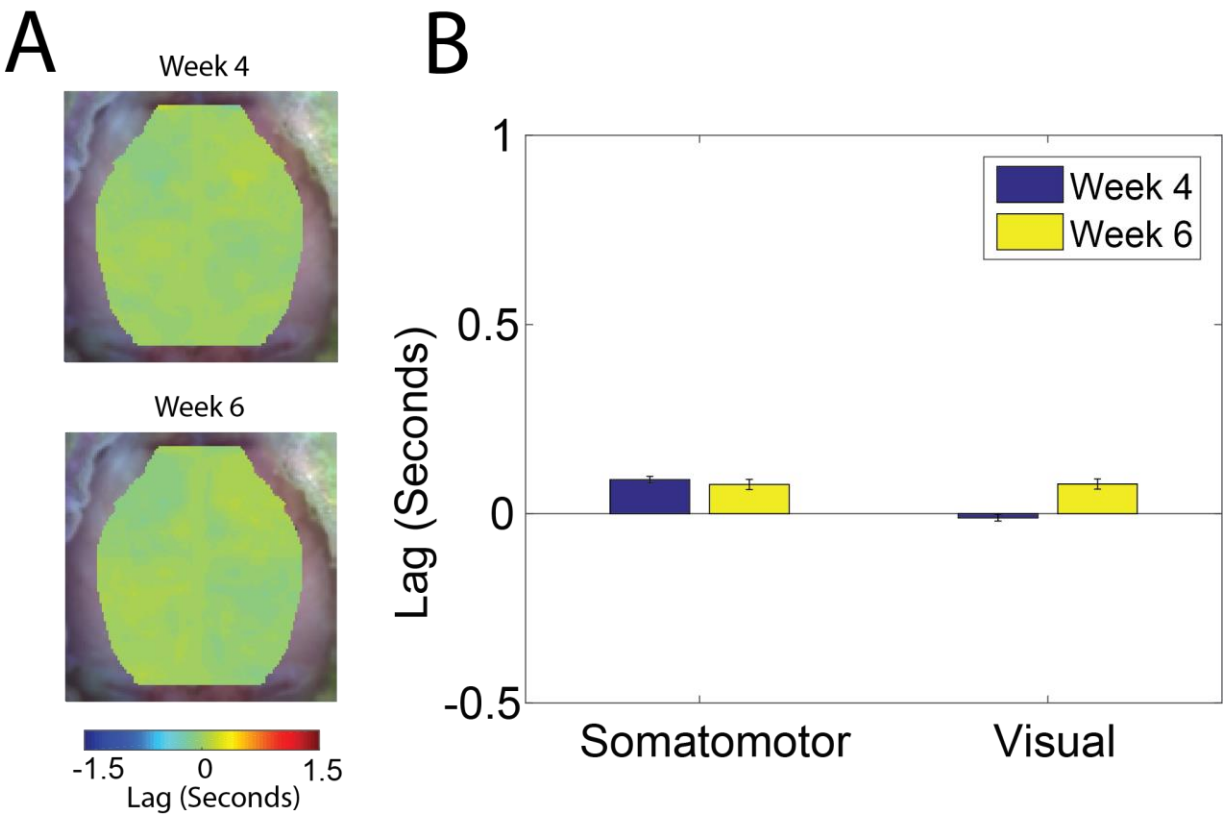


Fig. S13 – Homotopic lags in sham mice. A) Group average homotopic lag maps for sham injected mice (n=20) at week 4 and week 6 post injection. B) Quantification of the group average homotopic lag (n=20) for the somatosensory forelimb and visual seeds. This graph indicates that hemodynamic lag in the between the homotopic regions assessed are unchanged with the passage of time in our mouse model.